第 35 卷第 4 期
2019 年 4 月

无 机 化 学 学 报
CHINESE JOURNAL OF INORGANIC CHEMISTRY

Vol.35 No.4
695-702

一步醇–水热法合成高效的 F 掺杂 $BiVO_4$ 光催化剂

蒋海燕[1] 张 钒[1] 于曙光*,[1] 李育珍*,[2]
([1]青岛农业大学化学与药学院,青岛 266109)
([2]太原理工大学环境科学与工程学院,太原 030024)

摘要:以 NH_4F 为掺杂前体,采用简单的一步醇–水热法制备了 F 掺杂 $BiVO_4$ 光催化剂。利用 X 射线衍射(XRD)、扫描电子显微镜(SEM)、X 射线光电子能谱(XPS)、紫外–可见漫反射光谱(UV-Vis)和光致发光光谱(PL)表征了这些光催化剂的物理化学性质。在少量 H_2O_2 存在条件下,以可见光照射下光催化降解苯酚的反应测定了这些光催化剂的催化活性。研究表明,相较于未掺杂的 $BiVO_4$ 样品而言,F 掺杂 $BiVO_4$ 样品不仅仍保留了单斜结构,而且有更高的结晶度、表面氧空位密度和光生电荷载流子分离效率,更强的光吸收和更低的带隙能。在这些 F 掺杂 $BiVO_4$ 样品中,以 n_F/n_{Bi} 的理论值为 1.0 且带隙能为 2.43 eV 的 F 掺杂 $BiVO_4$ 样品的光催化活性最好(90 min 内苯酚的降解率可达 95%)。这一优良的光催化性能与其具有最高的结晶度、表面氧空位密度和光生电荷载流子分离效率,最强的光吸收和最低的带隙能有关。

关键词:一步醇–水热法;F 掺杂 $BiVO_4$;光催化;苯酚;光降解
中图分类号:O614.53 **文献标识码**:A **文章编号**:1001-4861(2019)04-0695-08
DOI:10.11862/CJIC.2019.074

Efficient F-Doped $BiVO_4$ Photocatalyst Synthesized by One-Step Alcohol-Hydrothermal Method

JIANG Hai-Yan[1] ZHANG Fan[1] YU Shu-Guang*,[1] LI Yu-Zhen*,[2]
([1]*College of Chemistry and Pharmaceutical Sciences, Qingdao Agricultural University, Qingdao, Shandong* 266109, *China*)
([2]*College of Environmental Science and Engineering, Taiyuan University of Technology, Taiyuan* 030024, *China*)

Abstract: F-doped $BiVO_4$ photocatalysts were fabricated by using a simple one-step alcohol-hydrothermal method with NH_4F as the precursor of the dopant. The physicochemical properties of the photocatalysts were characterized by X-ray diffraction (XRD), scanning electron microscopy (SEM), X-ray photoelectron spectroscopy (XPS), ultraviolet-visible diffuse reflectance spectroscopy (UV-Vis), and photoluminescence spectra (PL). Their photocatalytic activities were determined through the degradation of phenol in the presence of a small amount of H_2O_2 under visible-light illumination. It is found that compared to the un-doped $BiVO_4$ sample, the F-doped $BiVO_4$ samples retained the monoclinic structure and had higher crystallinity, surface oxygen vacancy densities and separation efficiency of photogenerated charge carriers, stronger optical absorbance performances, and lower bandgap energies. Among these F-doped $BiVO_4$ samples, the F-doped $BiVO_4$ sample (nominal n_F/n_{Bi}=1.0, bandgap energy=2.43 eV) exhibited the best photocatalytic performance (the conversion of phenol up to 95% in 90 min), due to the highest crystallinity, surface oxygen vacancy density, and separation efficiency of photogenerated charge carriers, the strongest optical absorbance performance, and the lowest bandgap energy.

Keywords: one-step alcohol-hydrothermal method; F-doped $BiVO_4$; photocatalysis; phenol; photodegradation

收稿日期:2018-11-02。收修改稿日期:2019-01-01。
国家自然科学基金(No.21676028),山西省重点研发计划(一般)社会发展项目(No.201703D321009-5)和青岛农业大学博士基金(No.663/1113317,663/1118005)资助项目。
*通信联系人。E-mail:yushuguang_2000@163.com,liyuzhen123456@126.com

0 Introduction

In the past decades, nanoscaled semiconductor photocatalysts have been widely investigated for the applications in the fields such as solar energy conversion and the degradation of environmental pollutants[1-2]. To date, TiO_2 is the most popular photocatalyst for its high photocatalytic activity, good chemical stability, non-toxicity, and low cost. Unfortunately, TiO_2 has a large band gap of 3.2 eV and responds only to ultraviolet light, which greatly restricts its practical application for the low utilization of solar energy. Therefore, it is highly desirable to develop novel photocatalysts with visible-light-responding photocatalytic ability.

Among various novel visible-light-responding photocatalysts, monoclinic bismuth vanadate, with a relatively narrow band gap (~2.4 eV), is considered as an important visible-light-driven semiconductor photocatalyst due to its exceptional optical and electronic properties, chemical stability and non-toxicity properties[3]. It has been used in organic pollutants degradation[4-5] and water splitting under visible light irradiation[6-7]. A number of studies have been focused on the controlled preparation of the effective monoclinic $BiVO_4$ photocatalyst with special morphology, high surface area, or exposed high-energy facets[4-8]. The photocatalytic performance of the individual $BiVO_4$, however, has not been ideal for practical application owing to the poor transportation and separation of photogenerated holes and electrons. Many methods have been used to enhance the photocatalytic performance of a photocatalyst, such as the fabrication of the upconversion nanoparticles based hetero-structures[9-11], hollow nanostructures[12], and pyroelectric materials[13]. According to some reports[14-16], the photocatalytic performance of $BiVO_4$ would be greatly increased by doping $BiVO_4$ with nonmetal atoms for the effective reduction of the recombination rate of photo-induced electron-hole pairs. For example, Wang et al.[14] synthesized N-doped $BiVO_4$ by using the complexing sol-gel method and observed that N-doped $BiVO_4$ exhibits the enhanced photocatalytic performance in the degradation of methyl orange under visible light irradiation. Guo et al.[15] found that in the degradation of methylene blue under visible light illumination, the photocatalytic activity of S-doped $BiVO_4$ photocatalyst is much higher than that of $BiVO_4$ photocatalyst because an appropriate amount of S^{2-} ions effectively improve the separation efficiency of photogenerated electron-hole pairs. Yin et al.[16] fabricated C-doped $BiVO_4$ photocatalyst with fine hierarchical structures using a novel sol-gel method, showing extremely high photocatalytic performance in O_2 production from water splitting under visible light irradiation.

Recently, our group[17] and Li et al.[18] have synthesized F-$BiVO_4$ using the two-step hydrothermal strategy, however, the method is complicated. Herein, in this study, we have prepared fluorine doped $BiVO_4$ material by using a simple one-step alcohol-hydrothermal method. The F-$BiVO_4$ samples show better photocatalytic activity toward the degradation of phenol under visible-light irradiation than the as-prepared $BiVO_4$ samples.

1 Experimental

1.1 Preparation of photocatalyst

F-doped $BiVO_4$ photocatalysts were fabricated using the alcoho-hydrothermal method with $Bi(NO_3)_3 \cdot 5H_2O$ and NH_4VO_3 as inorganic source, dodecylamine (DA) as surfactant, ethanol and ethylene glycol (EG) as solvent, and NH_4F as fluoride source. In a typical synthesis process, 5 mL of concentrated nitric acid (67%(*w*/*w*)) and 30 mmol of DA, were dissolved in a mixed solvent of 25 mL of ethanol and 25 mL of EG under stirring. $Bi(NO_3)_3 \cdot 5H_2O$ (10 mmol) and NH_4VO_3 (10 mmol) were added to the above mixed solution. Then the desired amount of NH_4F was added under stirring (nominal n_F/n_{Bi}=0.5, 1.0, and 1.5). When NH_4F was dissolved completely, a certain amount of NaOH solution (2 mol·L^{-1}) containing absolute ethanol and EG (V_{EOH}:V_{EG}=1) was used to adjust the pH value to 1.5. The final mixture was transferred into a 100 mL Teflon-lined stainless steel autoclave and maintained at 100 ℃ for 12 h. The precipitate was collected, washed three times with deionized water and absolute

ethanol, and then dried at 60 ℃ overnight. Finally, the powder was calcined in air at 450 ℃ for 4 h. The as-obtained material were named as $BiVO_4$, F-$BiVO_4$-0.5, F-$BiVO_4$-1, and F-$BiVO_4$-1.5 according to the nominal n_F/n_{Bi}, respectively.

All these chemicals (AR) were purchased from Beijing Chemicals Company and were used without further purification.

1.2 Characterization

The as-fabricated F-doped $BiVO_4$ catalysts were characterized by X-ray diffraction (XRD) using an X-ray diffractometer (Bruker/AXS D8 Advance) operated at 40 kV and 35 mA with a Cu $K\alpha$ X-ray radiation source and a nickel filter (λ=0.154 06 nm). Scanning electron microscopy (SEM) was performed on a Gemini Zeiss Supra 55 apparatus (operated at 10 kV). X-ray photoelectron spectroscopic (XPS) analysis was conducted on a Thermo Scientic K-Alpha, with Mg $K\alpha$ ($h\nu$=1 253.6 eV) as the excitation source. Ultraviolet-visible diffuse reflectance spectra (UV-Vis DRS) were measured with a Shimadzu UV-2450 spectrophotometer, using $BaSO_4$ as the reflectance standard. PL spectra were measured on an F-7000 fluorescence spectrometer at room temperature (wavelength of excitation light: 420 nm).

1.3 Photocatlytic activity tests

Photocatalytic activities of the as-prepared catalysts for the removal of phenol were evaluated in a quartz reactor (QO250, Beijing Changtuo Sci. & Technol. Co. Ltd.) under visible-light irradiation with a 300 W Xe lamp and a 400 nm cut-off filter. The photocatalytic process was conducted at RT as follows: 0.2 g of the as-prepared F-doped $BiVO_4$ sample and 0.6 mL of H_2O_2 solution (30%(w/w)) were added to an aqueous solution of phenol (200 mL, initial phenol concentration C_0=0.2 mmol·L^{-1}). Before illumination, the mixed solution was ultrasonicated for 0.5 h and then stirred for 3 h in the dark to establish the adsorption-desorption equilibrium of phenol on the surface of the samples. Then the reaction system was magnetically stirred and exposed to the visible-light irradiation. 5 mL of the suspension was collected at 15 min intervals and separated from the photocatalyst particles for analysis. The concentration (C_t) of phenol after reaction for some time was determined by monitoring the absorbance of phenol in the solution at *ca.* 280 nm during on the aforementioned UV-Vis equipment. The ratio (C_t/C_0) of phenol was used to evaluate the photocatalytic performance. All recycle photocatalytic tests were carried out under the same experimental conditions. The sample after every trial was collected by centrifugation, washed with a mixture of water and ethanol (1:1, V/V), and dried.

2 Results and discussion

2.1 Crystal structure

Fig.1 shows the XRD patterns of $BiVO_4$, F-$BiVO_4$-0.5, F-$BiVO_4$-1, and F-$BiVO_4$-1.5 samples. It is showed that all the peaks could be indexed as (110), (011), (121), (040), (200), (002), (211), (051), (240), (042), (202), (161), and (321) planes, which is in good agreement with that of pure monoclinic $BiVO_4$ (PDF No.14-0688) without impurities. It is seen that the doping of fluorine did not change the crystal type of

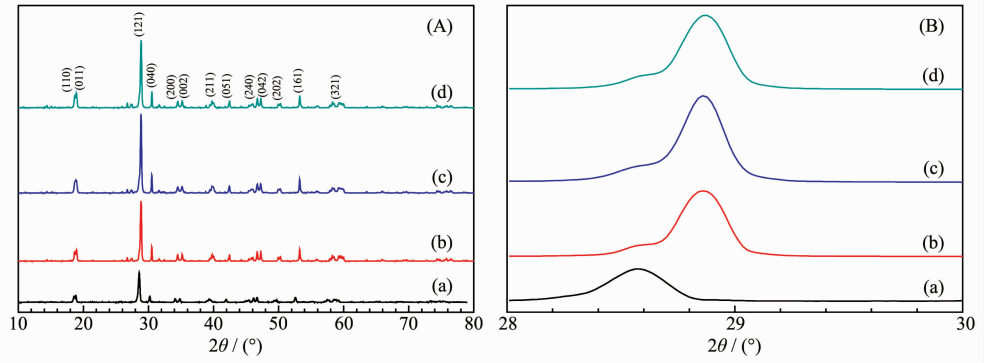

(a) $BiVO_4$, (b) F-$BiVO_4$-0.5, (c) F-$BiVO_4$-1, (d) F-$BiVO_4$-1.5

Fig.1 XRD patterns (A) and the magnified XRD patterns at 2θ=28°~30° (B) of as-fabricated samples

the $BiVO_4$ sample. A similar result was also reported by Li and his coworkers[18]. The diffraction peaks of F-$BiVO_4$-0.5, F-$BiVO_4$-1, and F-$BiVO_4$-1.5 samples were sharp and intense, indicating the highly crystalline character of these samples. As a result, the average crystalline size of the samples calculated according to the line width of the (121) diffraction peak based on the Scherrer formula were 29, 33, 36 and 35 nm, corresponding to $BiVO_4$, F-$BiVO_4$-0.5, F-$BiVO_4$-1, and F-$BiVO_4$-1.5, respectively. The crystalline sizes of the F-doped $BiVO_4$ samples were slightly bigger than that of $BiVO_4$ sample, attributed to a slight lattice distortion in the F-doped $BiVO_4$ samples[14]. In addition, from Fig.1(B), it can be seen that the (121) diffraction peak in the XRD patterns of F-doped $BiVO_4$ samples showed an obvious shift towards the higher diffraction angle, indicating the presence of compressive strain in the F-doped $BiVO_4$ samples[19].

2.2 Particle morphology

Fig.2 shows the SEM images of pure $BiVO_4$ sample and F-doped $BiVO_4$ samples. From Fig.2, an olive-like structure with a porous structure is observed for the $BiVO_4$, F-$BiVO_4$-0.5 and F-$BiVO_4$-1 samples. There were numerous mesopores and macropores on the surface of the olive-like particles. It can be demonstrated that the doping of the small amount of F had little effect on the morphology of the $BiVO_4$ samples. Similar phenomenon was also observed in the citric acid assisted preparation of the B-doped samples[20]. However, the F-$BiVO_4$-1.5 sample was composed of nano-sized particles and the olive-like micro-particles, indicating that the excess doping of fluorine could change the particle morphology of the $BiVO_4$ sample.

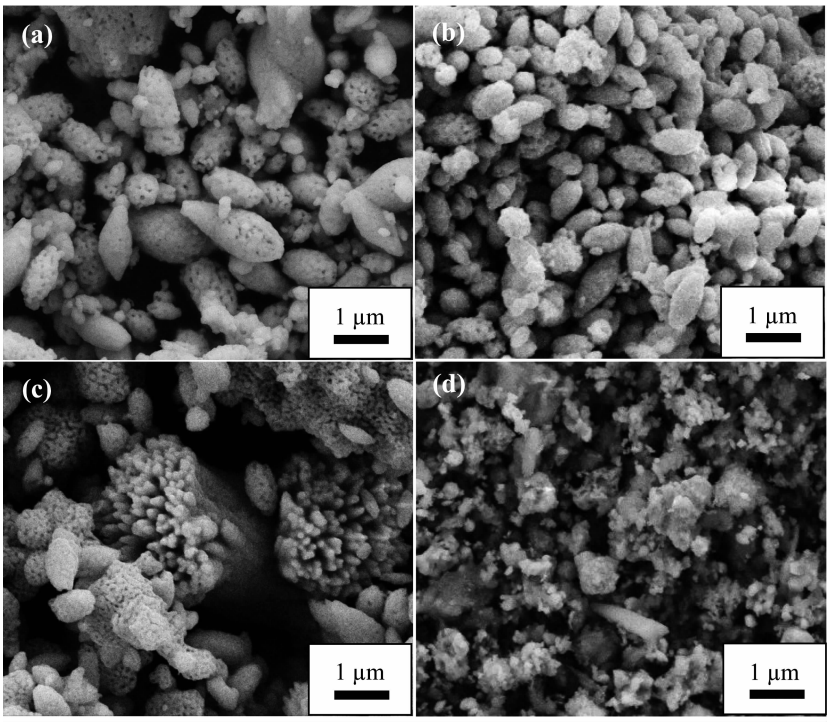

(a) $BiVO_4$, (b) F-$BiVO_4$-0.5, (c) F-$BiVO_4$-1, (d) F-$BiVO_4$-1.5

Fig.2 SEM images of as-fabricated samples

2.3 XPS analysis

In order to certify the doping of fluorine, XPS was performed to study the surface composition of $BiVO_4$ sample and F-$BiVO_4$-1 sample, as shown in Fig.3. From Fig.3(A), it can be seen that the Bi4*f* spectra of the as-obtained samples were consisted of two symmetrical peaks at binding energy (BE)=158.5 and 163.9 eV, corresponding to Bi4$f_{7/2}$ and Bi4$f_{5/2}$ signals respectively, which were characteristic of the Bi^{3+} species[21]. It can be concluded that the doping of fluorine had no effect on the chemical state of Bi. In Fig.3(B), the asymmetric peaks of V2$p_{3/2}$ were decom-

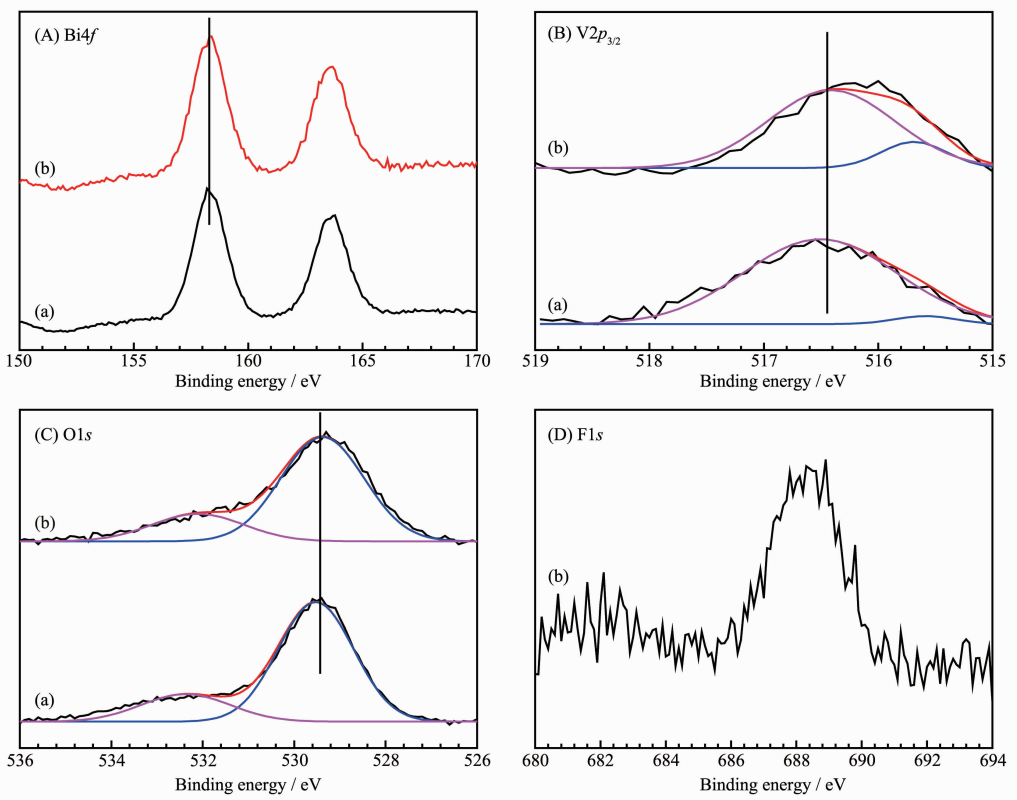

Fig.3　XPS spectra of Bi4*f* (A), V2$p_{3/2}$ (B), O1*s* (C) and F1*s* (D) of $BiVO_4$ sample (a) and F-$BiVO_4$-1 sample (b)

posed into two peaks with Gaussian distributions for the $BiVO_4$ sample and the F-$BiVO_4$-1 sample at BE= 515.5 and 516.4 eV, attributable to the surface of V^{4+} (in minority) and V^{5+} (in majority) species of the two samples[22]. The molar ratio of V^{4+} to V^{5+} (0.31) of F-$BiVO_4$-1 sample was higher than that (0.12) of $BiVO_4$ sample. According to the electro-neutrality principle, the as-prepared samples were oxygen-deficient and the amount of nonstoichiometric oxygen on the surface was dependent on the surface molar ratios ($n_{V^{4+}}/n_{V^{5+}}$). From Fig.3(C), it can be seen that the asymmetric O1*s* were deconvoluted into two components at BE=529.1 eV (in majority) and 532.1 eV (in minority), which could be assigned to surface lattice oxygen (O_{latt}) and adsorbed oxygen (O_{ads}) species, respectively[23-24]. The molar ratios of n_{Oads}/n_{Olatt} in $BiVO_4$ sample and F-$BiVO_4$-1 sample were 0.27 and 0.50, respectively. Therefore, the F-doped $BiVO_4$ sample contained more surface oxygen vacancies than the un-doped $BiVO_4$ sample, which could be helpful for the enhancement of the photocatalytic activity of $BiVO_4$ samples, as confirmed by the activity data shown later. From Fig.3 (D), the strong symmetric peak at BE=688.0 eV could be assigned to the fluorine ions in the lattice [25], indicating that the fluorine ions could be doped in the lattice of $BiVO_4$ crystal by the simple one-step alcohol-hydrothermal method.

2.4　Optical absorption behavior

The optical properties of the as-obtained samples were characterized by UV-Vis DRS, as shown in Fig. 4. According to Fig.4, all of the samples displayed strong absorption in the UV and visible light regions. It is clear that the absorption intensity of the F-doped $BiVO_4$ samples was stronger than the un-doped $BiVO_4$ sample, indicating that the F-doped $BiVO_4$ samples could better respond to visible light. A similar phenomenon was also observed by Shan and his coworkers[26]. The band gap could be determined by the Kubelka-Munk equation: $\alpha h\nu = A(h\nu - E_g)^{n/2}$, where α, A, $h\nu$, and E_g are the absorption coefficient, a constant, the discrete photon energy, and the band gap. The value of n depends on the characteristics of the transition in the semiconductor (n=1 for direct transition and n=4 for indirect transition). For $BiVO_4$,

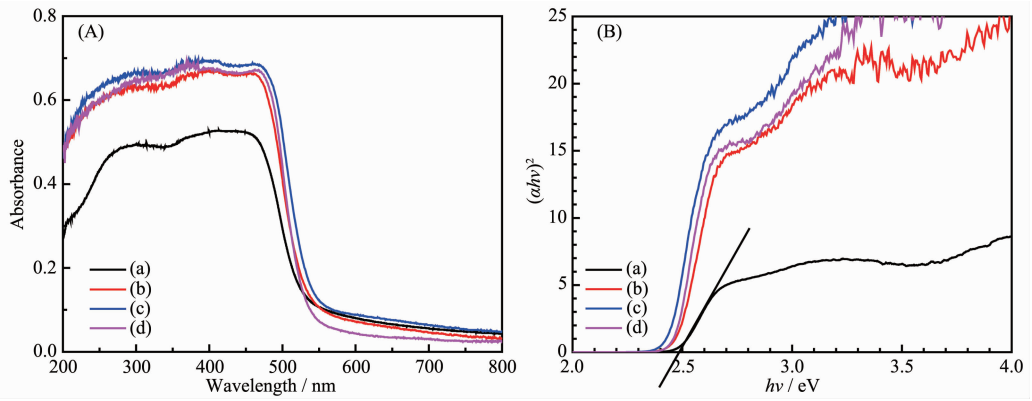

Fig.4 UV-Vis diffuse reflectance spectra (A) and plots of $(\alpha h\nu)^2$ versus $h\nu$ (B) of $BiVO_4$ (a), F-$BiVO_4$-0.5 (b), F-$BiVO_4$-1 (c) and F-$BiVO_4$-1.5 (d)

the value of n is 1. Fig.4 (B) presents the plots of $(\alpha h\nu)^2$ versus $h\nu$ of the as-prepared samples, the band gaps (E_g) of $BiVO_4$ sample, F-$BiVO_4$-0.5 sample, F-$BiVO_4$-1 sample and F-$BiVO_4$-1.5 sample were estimated to be 2.48, 2.46, 2.43 and 2.44 eV, respectively. Compared to the un-doped $BiVO_4$ sample, the band gaps of fluorine doped $BiVO_4$ samples decreased slightly. In accordance with XRD and XPS analysis, the result might be due to the increased oxygen vacancies in the F-doped $BiVO_4$ samples[27].

2.5 PL spectra

Effective separation of photogenerated charge carriers is an important factor for excellent photocatalytic activity of the photocatalyst. PL spectra are helpful to determine the separation efficiency of the photogenerated charge carriers. As shown in Fig.5, a broad PL peak centered at 530 nm could be observed for all the samples, however, the PL intensities of F-doped $BiVO_4$ samples were lower than that of $BiVO_4$ sample, indicating that the doping of fluorine could inhibit the recombination of photogenerated charge carriers and hence enhance the photocatalytic performance of $BiVO_4$ photocatalyst[28]. The result would be confirmed by the following photocatalytic activity tests.

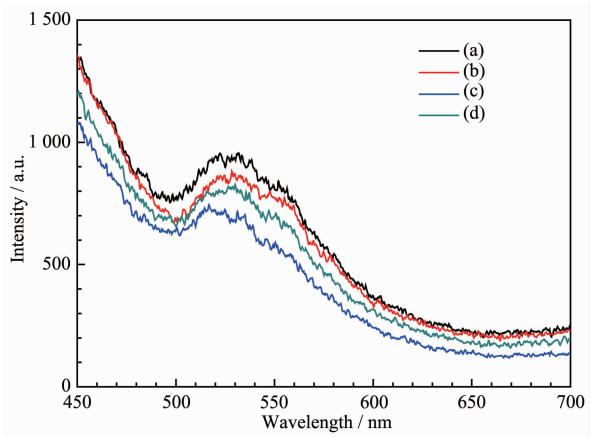

(a) $BiVO_4$, (b) $BiVO_4$-F-0.5, (c) $BiVO_4$-F-1, (d) $BiVO_4$-F-1.5

Fig.5 Room-temperature PL spectra of as-fabricated samples

2.6 Photocatalytic performance

To demonstrate the photocatlytic performance of fluorine doped $BiVO_4$ materials, the photocatalytic degradation of phenol in the presence of a small amount of H_2O_2 under visible light irradiation were investigated, as shown in Fig.6. It should be noticed that after visible light illumination for 90 min, the concentration of phenol in the presence of H_2O_2 was not changed and the conversion of phenol was only 8% over the F-$BiVO_4$-1 catalyst without H_2O_2. The F-doped $BiVO_4$ sample, however, showed high photocatalytic performance in the presence of H_2O_2 under visible light irradiation. It is indicated that there is a synergistic effect between H_2O_2 and the photocatalyst. H_2O_2, as an efficient electron scavenger, could trap the photoinduced electrons and inhibit the recombination of photoinduced electrons and photoinduced holes[29]. After irradiation for 90 min, nearly 95% of phenol was degraded by the F-$BiVO_4$-1 sample, while the other samples, including the pure $BiVO_4$ sample, F-$BiVO_4$-0.5 sample and F-$BiVO_4$-1.5 sample, exhibited lower degradation rates of *ca.* 77%, 90% and 92%, respectively. Compared with the un-doped $BiVO_4$

sample, all of the F-doped $BiVO_4$ samples showed an obvious enhancement on the photodegradation of phenol, due to higher molar ratios of $n_{V^{4+}}/n_{V^{5+}}$, more oxygen vacancy densities, and higher separation efficiency of photogenerated charge carriers of the F-doped $BiVO_4$ samples than those of the un-doped $BiVO_4$ sample, as confirmed by XPS and PL analysis. Furthermore, the F-doped $BiVO_4$ samples had stronger light absorption in the visible light region and lower ban-gap energies than the un-doped $BiVO_4$ sample, which might also contribute to the enhanced photocatalytic performance of fluorine-doped $BiVO_4$ samples.

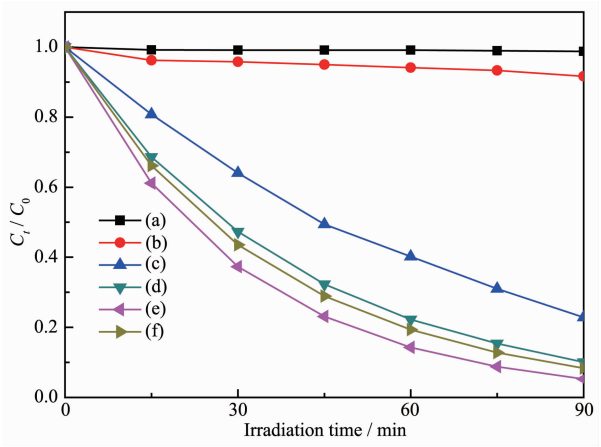

C_0=0.2 mmol·L^{-1}

Fig.6　Phenol concentration versus visible-light irradiation time for degradation of phenol aqueous solution under visible-light (≥400 nm) irradiation: (a) direct photolysis in the presence of H_2O_2; (b) F-$BiVO_4$-1 in the absence of H_2O_2; (c) $BiVO_4$, (d) $BiVO_4$-F-0.5, (e) $BiVO_4$-F-1 and (f) $BiVO_4$-F-1.5 in the presence of H_2O_2

To investigate the photostability of the fluorine-doped $BiVO_4$ photocatalyst in the photocatalytic reaction under visible light irradiation, the recycle experiments were performed. Fig.7 displays the results of three successive runs for the photodegradation of phenol over F-$BiVO_4$-1 photocatalyst under the identical experimental conditions. As can be seen in Fig.7, the photocatalytic performance of F-$BiVO_4$-1 photocatalyst did not exhibited a significant loss after three successive runs, indicating the excellent

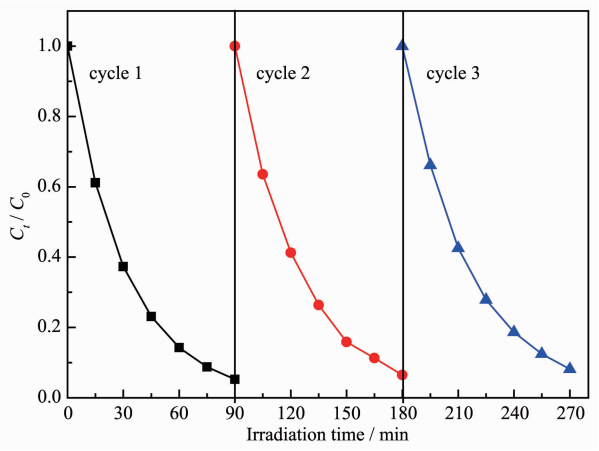

Fig.7　Recycling test on F-$BiVO_4$-1 photocatalyst for degradation of phenol under visible light irradiation

photostability of F-doped $BiVO_4$ photocatalyst under visible light illumination.

2.7　Photocatalytic mechanism

The photocatalytic experiments were performed with assistance of H_2O_2 to achieve efficient degradation of phenol. The hydroxyl radicals (·OH), deriving from the decomposition of H_2O_2, are efficient active species to oxidize phenol[30]. Under visible-light irradiation, F-$BiVO_4$ photocatalyst is inspired to generate photo-generated carries. The electrons from the valence band (VB) are transferred to the conduction band (CB), leaving lots of holes in VB. The photo-generated holes react with surface hydroxyl to form ·OH radicals[31]. The photo-generated electrons react with absorbed O_2 on the surface of photocatalyst or dissolved O_2 in water to generate $\cdot O_2^-$ radicals. The photo-generated electrons might also reacted with H_2O_2 to produce ·OH radicals[30]. ·OH and $\cdot O_2^-$ radicals with strong oxidation ability are responsible for the degradation of phenol. The main reaction steps for the photodegra-dation of phenol in addition of H_2O_2 under visible-light irradiation might be proposed as Eq.(**1**)~(**6**).

$$\text{F-BiVO}_4 + h\nu \rightarrow \text{F-BiVO}_4\ (e_{CB}^-) + \text{F-BiVO}_4\ (h_{VB}^+) \quad (\mathbf{1})$$

$$\text{F-BiVO}_4\ (h_{VB}^+) + OH^- \rightarrow \cdot OH + \text{F-BiVO}_4 \quad (\mathbf{2})$$

$$\text{F-BiVO}_4\ (e_{CB}^-) + H_2O_2 \rightarrow 2\cdot OH + \text{F-BiVO}_4 \quad (\mathbf{3})$$

$$\text{F-BiVO}_4\ (e_{CB}^-) + O_2 \rightarrow \cdot O_2^- + \text{F-BiVO}_4 \quad (\mathbf{4})$$

$$\cdot OH + \text{phenol} \rightarrow \text{Degraded products} \quad (\mathbf{5})$$

$$\cdot O_2^- + \text{phenol} \rightarrow \text{Degraded products} \quad (\mathbf{6})$$

3 Conclusions

In summary, fluorine-doped $BiVO_4$ photocatalysts were prepared by adopting a simple one-step alcohol-hydrothermal strategy with NH_4F as fluorine source. It was found that the doping of fluorine do not change the crystal type of $BiVO_4$. Compared to the un-doped $BiVO_4$, the fluorine-doped $BiVO_4$ samples had higher crystallinity and separation efficiency of photogenerated charge carriers, more surface oxygen vacancy, stronger optical absorbance performance, and lower bandgap energy. The fluorine doped $BiVO_4$ sample with a nominal n_F/n_{Bi} of 1.0 and a bandgap energy of 2.43 eV exhibited excellent photocatalytic activity for the degradation of phenol in the presence of a small amount of H_2O_2 under visible-light illumination. The excellent photocatalytic activity of fluorine-doped $BiVO_4$ can be attributed to higher surface oxygen vacancy density and separation efficiency of photo-generated charge carriers, stronger optical absorbance performance, and lower bandgap energy.

Acknowledgements: The work was supported by the National Nature Science Foundation of China (Grant No. 21676028), the Shanxi Provincial Key Research and Development Plan (general) Social Development Project (Grant No.201703D321009-5), and the Scientific Research Foundation of Qingdao Agricultural University (Grants No.663/1113317, 663/1118005).

References:

[1] Xin X, Lang J Y, Wang T T, et al. *Appl. Catal. B*, **2016**,**181**: 197-209

[2] Zhao D, Wu Q, Yang C F, et al. *Appl. Surf. Sci.*, **2015**,**356**: 308-316

[3] Li Y, Sun Z H, Zhu S M, et al. *Carbon*, **2015**,**94**:599-606

[4] Zhang X F, Du L L, Wang H, et al. *Microporous Mesoporous Mater.*, **2013**,**173**:175-180

[5] Ji K M, Dai H X, Deng J G, et al. *Appl. Catal. B*, **2015**,**168-169**:274-282

[6] Hernández S, Thalluri S M, Sacco A, et al. *Appl. Catal. A*, **2015**,**504**:266-271

[7] Thalluri S M, Suarez C M, Hernández S, et al. *Chem. Eng. J.*, **2014**,**245**:124-132

[8] Thalluri S M, Hussain M, Saracco G, et al. *Ind. Eng. Chem. Res.*, **2014**,**53**(7):2640-2646

[9] Zhang F, Zhang C L, Wang W N, et al. *ChemSusChem*, **2016**, **9**(12):1449-1454

[10]Wang W N, Huang C X, Zhang C Y, et al. *Appl. Catal. B*, **2018**,**224**:854-862

[11]LI Yao-Wu(李耀武), HUANG Chen-Xi(黄辰曦), TAO Wei (陶伟), et al. *Chinese J. Inorg. Chem.*(无机化学学报), **2017**, **33**(3):361-376

[12]Zhang C Y, Liu H H, Wang W N, et al. *Appl. Catal. B*, **2018**,**239**:309-316

[13]Xu X L, Xiao L B, Jia Y M, et al. *Energy Environ. Sci.*, **2018**,**11**:2198-2207

[14]Wang M, Liu Q, Che Y S, et al. *J. Alloys Compd.*, **2013**, **548**:70-76

[15]Guo M N, Wang Y, He Q L, et al. *RSC Adv.*, **2015**,**5**:58633 -58639

[16]Yin C, Zhu S M, Chen Z X, et al. *J. Mater. Chem. A*, **2013**, **1**:8367-8378

[17]Jiang H Y, Dai H X, Deng J G, et al. *Solid State Sci.*, **2013**, **17**:21-27

[18]Li J Q, Guo Z Y, Liu H, et al. *J. Alloys Compd.*, **2013**,**581**: 40-45

[19]Jagadale T C, Takale S P, Sonawane R S, et al. *J. Phys. Chem. C*, **2008**,**112**(37):14595-14602

[20]Wang M, Zheng H Y, Liu Q, et al. *Spectrochim. Acta Part A*, **2013**,**114**:74-79

[21]Poulston S, Price N J, Weeks C, et al. *J. Catal.*, **1998**,**178** (2):658-667

[22]Liu W, Lai S Y, Dai H X, et al. *Catal. Lett.*, **2007**,**113**(3/4): 147-154

[23]Colón G, Hidalgo M C, Munuera G, et al. *Appl. Catal. B*, **2006**,**63**:45-59

[24]Kulkarni G U, Rao C N R, Roberts M W. *J. Phys. Chem.*, **1995**,**99**(10):3310-3316

[25]Yu J C,Yu J G, Ho W K, et al. *Chem. Mater.*, **2002**,**14**(9): 3808-3816

[26]Shan L W, Wang G L, Suriyaprakash J, et al. *J. Alloys Compd.*, **2015**,**636**:131-137

[27]Zhang A P, Zhang J Z. *Spectrochim. Acta Part A*, **2009**,**73** (2):336-341

[28]Tang J T, Liu Y H, Li H Z, et al. *Chem. Commun.*, **2013**, **49**:5498-5500

[29]Shang M, Wang W Z, Sun S M, et al. *J. Phys. Chem. C*, **2009**,**113**(47):20228-20233

[30]Wang Q L, Li H Y, Yang J H, et al. *Appl. Catal. B*, **2016**, **192**:182-192

[31]Zhu C S, Zheng J T, Fang L Y, et al. *J. Mol. Catal. A*: *Chem.*, **2016**,**424**:135-144